Composites: Part B 40 (2009) 417–426

Contents lists available at ScienceDirect

Composites: Part B

journal homepage: www.elsevier.com/locate/compositesb

Multiscale aggregating discontinuities method for micro–macro failure of composites

Jeong-Hoon Song *, Ted Belytschko

Theoretical and Applied Mechanics, Northwestern University, Evanston, IL 60208-3111, USA

ARTICLE INFO

Article history:
Received 4 December 2008
Accepted 27 January 2009
Available online 7 May 2009

Keywords:
A. Metal–matrix composites
B. Fracture
C. Finite element analysis
Mutiscale methods

ABSTRACT

The application of a multiscale method, called the multiscale aggregating discontinuities (MAD) method, to the failure analysis of composites is described. Two distinct features of the MAD method are the use of perforated unit cells, and the extraction of coarse-grained failure information. In the perforated unit cell, all subdomains of the unit cell that are not strictly elliptic are excluded, which enables the decomposition of its stable and unstable material. By means of these concepts, it is possible to compute an equivalent discontinuity at the macroscale, including both the direction and the magnitude of the discontinuity. This equivalent discontinuity is then passed to the macroscale along with the computed stress from the unit cell. The macroscale discontinuity is injected into the macro model by the extended finite element method (XFEM) procedure. In this paper, the method is improved by adding hourglass modes to the unit cell deformations, which better model growing cracks. Several examples comparing the MAD method with direct numerical simulations are presented.

1. Introduction

The modeling of failure in composites is one of the most challenging multiscale problems currently confronting the computational mechanics community. In the failure of composites, subscale failure can occur at several scales. For example, fiber–matrix separation and cracks in the matrix occur at much smaller scales than failure of the structure. In many cases, fibers are composed of fiber bundles, and the explication and quantification of their behavior requires an analysis at even smaller scales. Modeling of these various scales of response requires coarse-graining methods, for otherwise they are too expensive. Even in nanocomposites, where failure can be reduced to the atomistic scale as bond breaking, atomistic models cannot be used for modeling complete nanocomposite components. To treat these problems, it is necessary to have at hand computational multiscale methods which correctly coarse-grain failure so that this behavior can be incorporated in more efficient models.

The pre-failure behavior of composites has been treated quite effectively by classical homogenization techniques [1,2]. In these methods, the material behavior, i.e. the constitutive equation for the coarser scales, is obtained by solving a boundary value problem for a representative volume element (RVE). The RVE can be solved before undertaking the coarse scale analysis or concurrently with the macroscale model, as in the FE^2 [3,4]. Generally, these methods take advantage of a separation of scales between the scales of the RVE and the macro model.

In extending these methods to failure behavior, it is common to use damage theories in which the effect of microcracks is represented by damage parameters that represent the degradation of the material. When the damage variables become sufficiently large to cause one of the stress components to vanish, the material is considered to have failed. Such damage models are used both at the macroscale and subscales.

However, there are several theoretical shortcomings of these methods that call into question their viability. The main one is that once the stress–strain response of the RVE is no longer stable, the associated macro model is no longer well-posed. Stability is here meant in the sense of Hadamard and Hill (the equations are given later). Suffice it to say, that when the stress does not increase with increasing strain, e.g. in the presence of strain softening, material stability is often lost, and it is definitely lost in damage laws before one of the stress components goes to zero. The question of how to deal with this was a topic of great interest in the 1980s, when Bažant and Belytschko [5] showed that in a strain softening material, the strain vanishes on a set of measure zero and becomes infinite there. Many methods were proposed for dealing with this pathology: Bažant et al. [6] proposed a nonlocal model, Lasry and Belytschko [7] proposed gradient theories and studied their effects on the Liapunov coefficients, Chen and Schreyer [8] developed a nonlocal form of plasticity.

As a consequence, the multiscale modeling of failure requires a major revision of the homogenization approach. Once the

* Corresponding author.
E-mail address: j-song2@northwestern.edu (J.-H. Song).

1359-8368/$ - see front matter © 2009 Elsevier Ltd. All rights reserved.
doi:10.1016/j.compositesb.2009.01.007

material at the subscale has failed enough for the macroscale law to lose stability, it is no longer appropriate to simply pass the stress to the macroscale. Several investigators have already recognized this: Kouznetsova et al. [9] and Vernerey et al. [10,11] have used gradient theories. Oskay and Fish [12] have used the concept of eigendeformation to model cracks at various scales within the framework proposed in Fish and Yuan [13]. Other relevant works can be found in Raghavan and Ghosh [14] and Ghosh et al. [15].

In this paper, we further develop an alternative strategy based on aggregating discontinuities at the finer scales and passing these to the coarser scale. This method was first proposed in Belytschko et al. [16]. Its key features were the development of a perforated unit cell which excludes all subdomains of unstable material behavior such as cracking. It was shown that the resulting methodology insures the material stability at the coarser scale, and hence the well-posedness of the coarse scale problem. In addition, methods for extracting an equivalent discontinuity from the unit cell response were developed.

However, it was found that the conventional boundary conditions based on a constant deformation gradient were not effective in modeling the growth of a crack at the fine scale. Therefore in this paper, we further study an enhancement of the theory proposed in [17]; it consists of adding a so-called hourglass mode. It is shown that this mode fits well with the structure of four-node quadrilaterals with one-point quadrature and stabilization. We also shown how this method can be extended to atomistic models to probe nanoscale behavior.

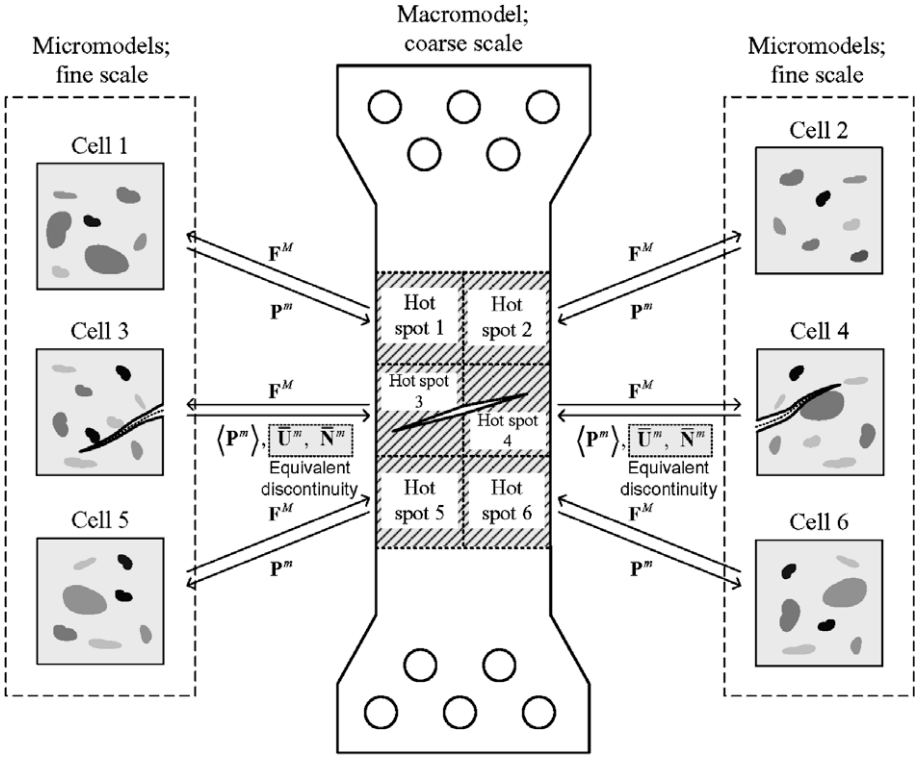

Fig. 1. Schematic of macro–micro linkages of the MAD method.

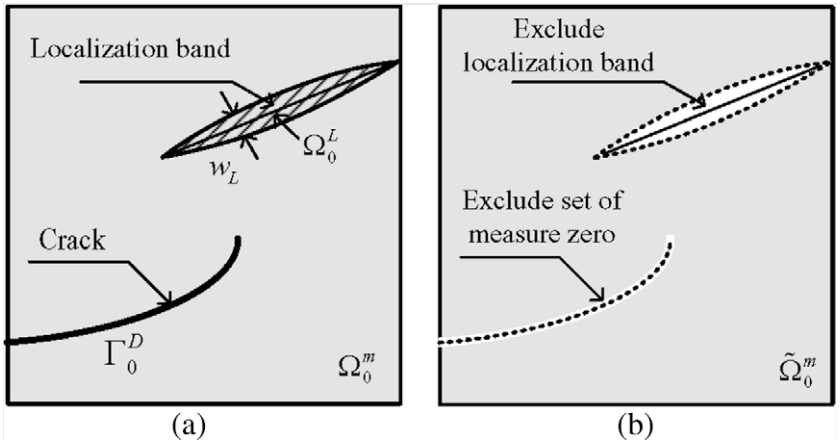

Fig. 2. Schematic of a perforated unit cell in a continuum scale model.

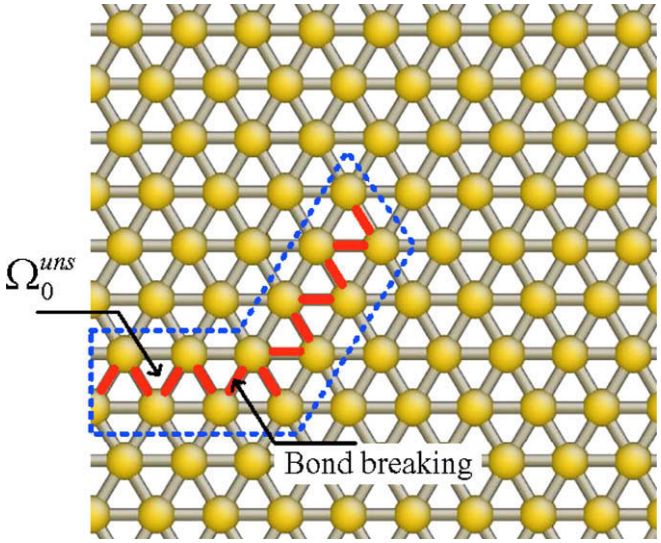

Fig. 3. Schematic of a perforated unit cell in an atomistic scale model.

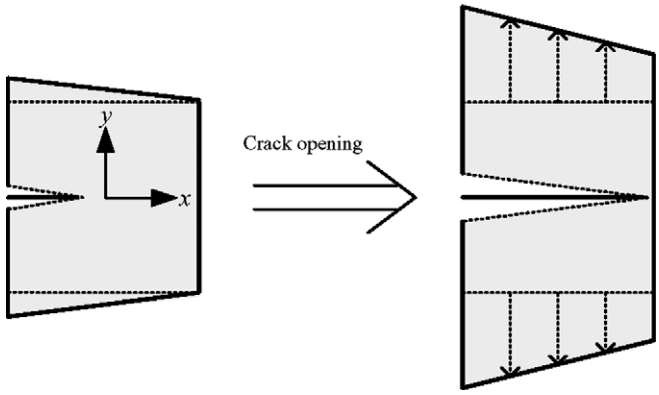

Fig. 5. Schematic illustrating how crack opening is dominated by the hourglass mode.

2. Coarse-graining method

A schematic of a typical macro–micro model for the MAD method is shown in Fig. 1. In the macro model which is modeled with coarse scale, so-called hot spots are linked with micro models; the micro models have fine-scale resolution and are calculated at the same time as the macro model as in the FE^2 method of Feyel and Chaboche [3] and Feyel [4]. The micro models can either be continuum models or atomistic models. For example, in Fig. 1, hot spots 1–6 in the macro model are linked with the unit cells. The macro model passes a measure of deformation to the linked unit cell, and then receives the computed stress and a description of the aggregated discontinuity from the unit cell; in our notation, superscript M refers to the macroscale, and m refers to the microscale. Note that cells 3 and 4 contain strong discontinuities, so the coarse-grained failure information within those unit cells is provided to the associated hot spots in the macro model; we will discuss this coarse-graining procedure subsequently.

The MAD method can be implemented in any conventional finite element software. In principle, the method is applicable to any elements, but, for the computations reported here, we used a one-point quadrature four-node quadrilateral element with hourglass control [18–20]. For the representation of strong discontinuities in macro and micro continuum models, we used the XFEM approach [21–23].

We employ two key concepts for coarse-graining failure phenomena [16]:

(1) all averaging operations are performed over a "perforated" unit cell that excludes all subdomains where the material loses strict ellipticity (these usually correspond to areas of material instability, including cracks),
(2) a single equivalent discontinuity, i.e. a coarse-grained discontinuity, is extracted from the discontinuous localized deformation and passed to the macroscale.

To clarify the first statement, we define material stability (ellipticity) and strict ellipticity. We make this definition in terms of the first Piola–Kirchhoff stress $\mathbf{P}$ and the deformation gradient $\mathbf{F}$. Consider a tangent matrix $\mathbf{C}$ which relates $\dot{\mathbf{P}}$ and $\dot{\mathbf{F}}$ (superposed dots denote material derivatives) by

$$\dot{\mathbf{P}} = \mathbf{C} : \dot{\mathbf{F}} \tag{1}$$

Then the material is strictly elliptic if

$$\mathbf{A} : \mathbf{C} : \mathbf{A} > 0 \quad \forall \mathbf{A} \tag{2}$$

Note that Eq. (2) also corresponds to the positive definiteness of $\mathbf{C}$.

A material is stable (often called rank-1 stable), and the governing equations are elliptic if

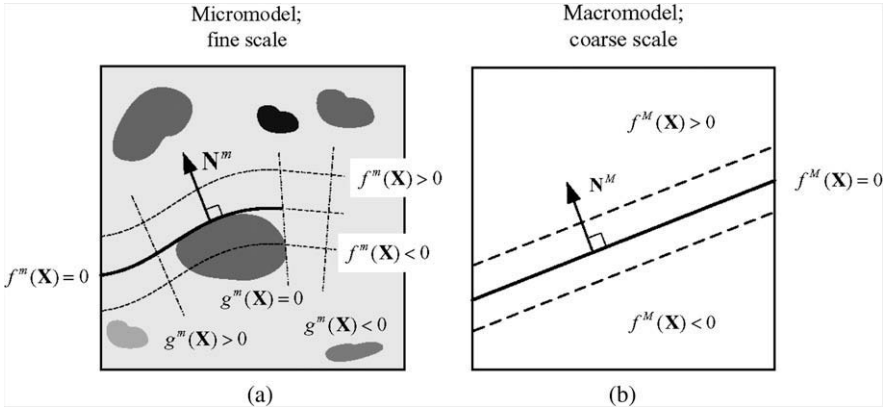

Fig. 4. Relation of cracks at the microscale and macroscale.

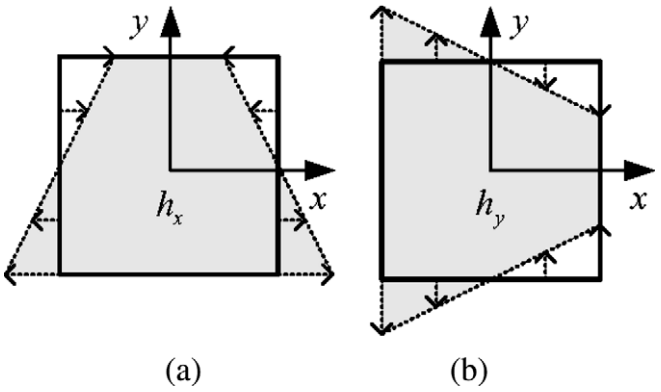

Fig. 6. Schematic of the hourglass modes: (a) x-direction hourglass mode, and (b) y-direction hourglass mode.

Table 1
Material properties of the aluminum–boron composite material.

Material	Young's modulus (GPa)	Poisson's ratio	Density (kg/m^3)
Aluminum	67.5	0.36	2700.0
Boron	413.0	0.20	2340.0
Homogenized material	75.6	0.35	2500.0

$$\boldsymbol{g}\otimes\boldsymbol{h}:\mathbf{C}:\boldsymbol{g}\otimes\boldsymbol{h}>0 \quad \forall \boldsymbol{g} \text{ and } \boldsymbol{h} \tag{3}$$

Note that Eq. (3) implies Eq. (2) when $\mathbf{C}$ is symmetric, i.e. that if a material is strictly elliptic, it is also stable and elliptic. Therefore, our perforated unit cell excludes some stable material. However, this does not appear to impair the performance of this method.

2.1. The perforated unit cell

We denote the reference domain for a unit cell of the microstructure at a point $\boldsymbol{X}$ by $\Omega_0^m(\boldsymbol{X})$ (usually the $\boldsymbol{X}$ will be dropped) and its boundary by $\partial\Omega_0^m$. The reference domain of the macrostructure is denoted by Ω_0^M and its boundary by $\partial\Omega_0^M$. A perforated unit cell that contains a crack Γ_0^D and a localization band Ω_0^L is shown in Fig. 2(a). The perforated unit cell is denoted by $\widetilde{\Omega}_0^m$ so

$$\widetilde{\Omega}_0^m = \Omega_0^m / \Omega_0^{uns} \tag{4}$$

where Ω_0^{uns} is the subdomain of the unit cell where the material loses strict ellipticity; i.e. $\Omega_0^{uns} = \Gamma_0^D \cup \Omega_0^L$.

A key attribute of this theory is that all averaging operations are performed over the perforated unit cell, so denoting the averaging operation by $\langle\cdot\rangle$, we have for any function $f(\boldsymbol{X})$:

$$\langle f(\boldsymbol{X})\rangle = \frac{1}{\left|\widetilde{\Omega}_0^m\right|}\int_{\widetilde{\Omega}_0^m} f(\boldsymbol{X})\mathrm{d}\Omega \tag{5}$$

where $|\cdot|$ denotes the measure of the domain, such as the area in two dimensions or the volume in three dimensions. Thus, for the

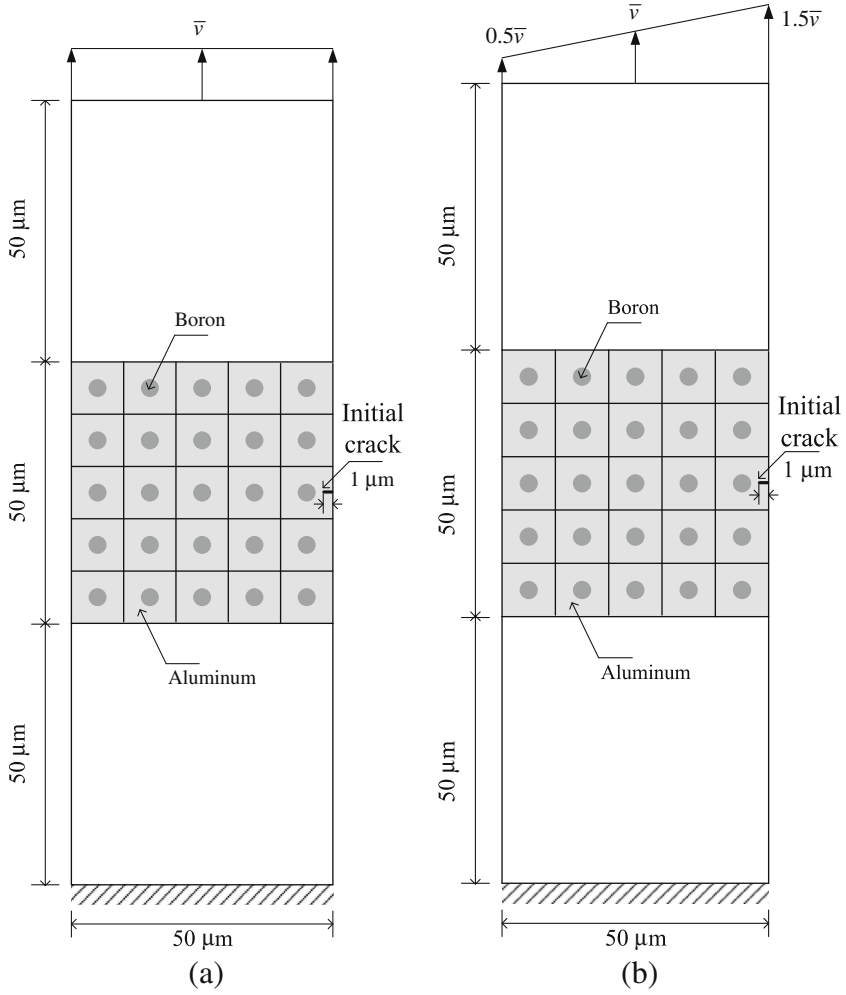

Fig. 7. Initial setups for one dimensional tests. Problem definitions for: (a) uniformly loaded rod, (b) rod with linearly varying velocity.

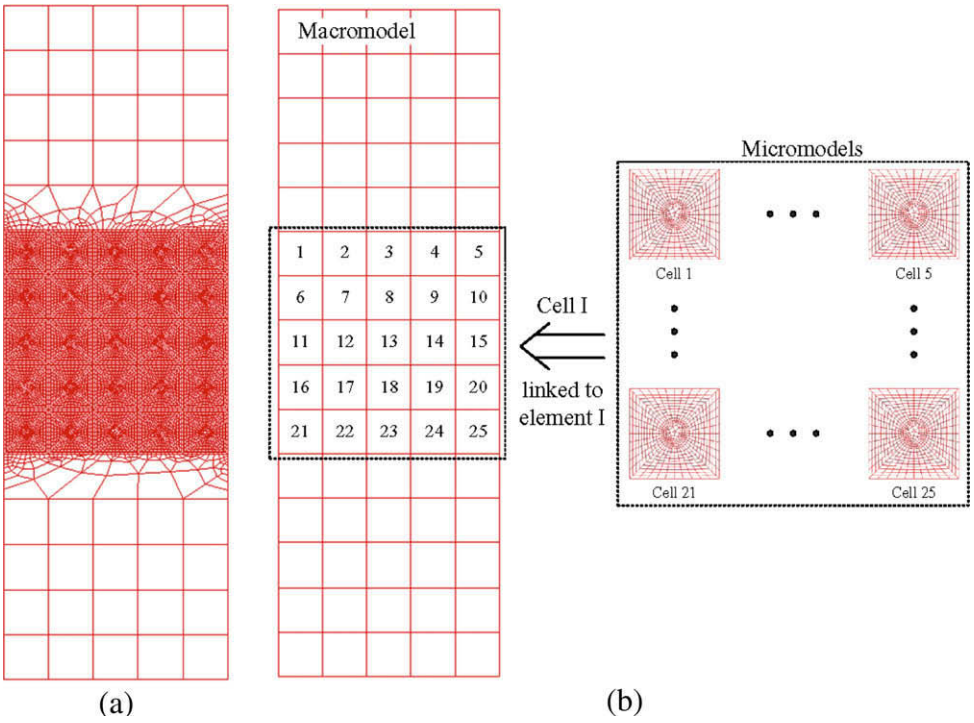

Fig. 8. Finite element discretizations for: (a) the direct numerical simulation, (b) the coarse-grained model and unit cell models for the MAD method.

deformation gradient $\mathbf{F}^m$ and first Piola–Kirchhoff stress $\mathbf{P}^m$, we have

$$\langle \mathbf{F}^m \rangle = \frac{1}{\left|\widetilde{\Omega}_0^m\right|} \int_{\widetilde{\Omega}_0^m} \mathbf{F}^m \mathrm{d}\Omega \tag{6}$$

$$\langle \mathbf{P}^m \rangle = \frac{1}{\left|\widetilde{\Omega}_0^m\right|} \int_{\widetilde{\Omega}_0^m} \mathbf{P}^m \mathrm{d}\Omega \tag{7}$$

For atomistic models, the averaged strain is computed by first fitting the displacements with a moving least square (MLS) approximation [24]. Let $\mathbf{u}_I$ be the atomistic displacements. The MLS approximation is then given

$$u_i = \sum_I N_I^{MLS}(\boldsymbol{X}) u_{iI} \tag{8}$$

where $N_I^{MLS}(X)$ is the MLS shape function. The deformation gradient at the atomistic scale is then given by

$$F_{ij}^m = \delta_{ij} + \sum_I \frac{\partial N_I}{\partial X_j} u_{iI} \tag{9}$$

To compute the stress, we use the virial stresses at the centers of the bonds

$$\mathbf{P}^m(\boldsymbol{X}_I) = \mathbf{F}^T((\boldsymbol{X}_I - \boldsymbol{X}_J) \otimes \boldsymbol{f}_{IJ}) \tag{10}$$

where $\boldsymbol{f}_{IJ}$ is the force in the bond connecting atoms I and J, and $\boldsymbol{X}_I$ and $\boldsymbol{X}_J$ are the coordinates of atom I and J, respectively. Then, compute the stress field by a MLS approximation

$$\mathbf{P}(\boldsymbol{X}) = \sum_I N_I^{MLS}(\boldsymbol{X}) \mathbf{P}(\boldsymbol{X}_I) \tag{11}$$

The bonds in which the force-field is such that bond force decreases with increasing elongation, and are therefore unstable, constitute the domain Ω_0^{uns}. For example, consider the model shown in Fig. 3. For the stage in crack growth where the bonds shown in red are unstable, the domain Ω_0^{uns} encompasses all of these bonds. The domain Ω_0/Ω_0^{uns} is the remainder of the domain and is used in the calculation of the average stress $\langle \mathbf{P}^m \rangle$.

The macrocrack can be an approximation to either a single crack or a group of cracks at the microscale. However, in this paper, we only consider a single crack at the microscale, so it can be described by

$$f^m(\boldsymbol{X}) = 0 \quad \text{and} \quad g^m(\boldsymbol{X}) > 0 \tag{12}$$

where $f^m(\boldsymbol{X}) = 0$ is a level set that describes the surface of the crack and $g^m(\boldsymbol{X}) > 0$ describes its extent. The crack path at the microscale may be jagged, but it is assumed that the crack path penetrates the

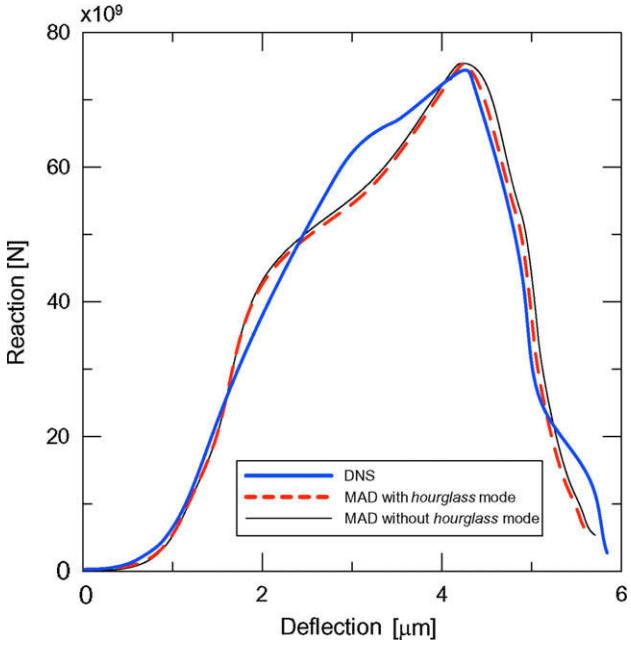

Fig. 9. The comparison of load–deflection curves between the DNS and the MAD method with and without the hourglass mode.

walls of the unit cell at no more than two points. The crack front is given by

$$f^m(\boldsymbol{X}) = g^m(\boldsymbol{X}) = 0 \tag{13}$$

A typical crack at the microscale and its macroscale equivalent is shown in Fig. 4. The geometry of the equivalent macrocrack in a neighborhood corresponding to the unit cell is described by an affine level set function

$$f^M(\boldsymbol{X}) = \alpha_0 + \alpha_\beta X_\beta = 0 \tag{14}$$

where α_0 and α_β are arbitrary parameters.

The motion $\phi^m(\boldsymbol{X})$ on the outside surfaces of the unit cell given by

$$\phi^m(\boldsymbol{X}) = \mathscr{F}^M \cdot \boldsymbol{X} + \boldsymbol{q}XY \quad \text{on } \boldsymbol{X} \in \Gamma^m \tag{15}$$

where in two dimensions $\boldsymbol{q}^T = [q_x\ q_y]$. The last term in Eq. (15) accounts for the hourglass modes; $\boldsymbol{q}$ is obtained from the macroscale deformation as described later. This last term is one of the key differences from the previously presented MAD method [16]. However, this term has no effect on the discontinuity. Therefore, as in [16], we can obtain the approximate discontinuity by

$$(\overline{\mathbf{U}}, \overline{\mathbf{N}}) = \arg\left(\min_{\overline{\mathbf{U}}, \overline{\mathbf{N}}} \left(\overline{\mathbf{U}} \otimes \overline{\mathbf{N}} - \mathscr{F}^M + \langle \mathbf{F}^m \rangle \right)^2 \right) \tag{16}$$

where the jump in the displacement at the macroscale is given by

$$[\![\phi^M]\!] = \frac{\left|\widetilde{\Omega}_0^m\right|}{R} \overline{\mathbf{U}} \tag{17}$$

where R is a characteristic dimension of the unit cell.

2.2. Representation of crack opening in unit cells

When a crack opens and grows in a unit cell, the unit cell undergoes deformations such as that shown in Fig. 5. This mode of deformation cannot be effectively represented by a constant deformation gradient. In crack opening, the deformation of the boundaries of the unit cell are bilinear, often called an hourglass mode in the finite element literature. Effective modeling of crack growth requires that the hourglass mode be included in the deformation of the unit cell.

Here, we will briefly describe a numerical scheme which allows us to extract the hourglass mode from the coarse scale model that is discretized with four-node quadrilateral elements; the hourglass modes for a four-node quadrilateral element are shown in Fig. 6. These schemes are based on Flanagan and Belytschko [18], and Belytschko and Bachrach [20].

The hourglass mode displacement at the center of four-node quadrilateral element can be computed by

$$\boldsymbol{q} = \boldsymbol{u}_I \gamma_I \tag{18}$$

where $\boldsymbol{u}_I$ is the nodal displacement of the finite element, and γ_I is the hourglass mode projection operator. The hourglass mode projection operator is defined by

$$\gamma_I = \frac{1}{4}(\boldsymbol{h}_I - (\boldsymbol{h}_J \boldsymbol{x}_J)\boldsymbol{b}_{xI} - (\boldsymbol{h}_J \boldsymbol{x}_J)\boldsymbol{b}_{yI}) \tag{19}$$

where $\boldsymbol{x}_I$ is the current nodal coordinates of the finite element, and $\boldsymbol{h}$ and $\boldsymbol{b}$ are defined, respectively, as

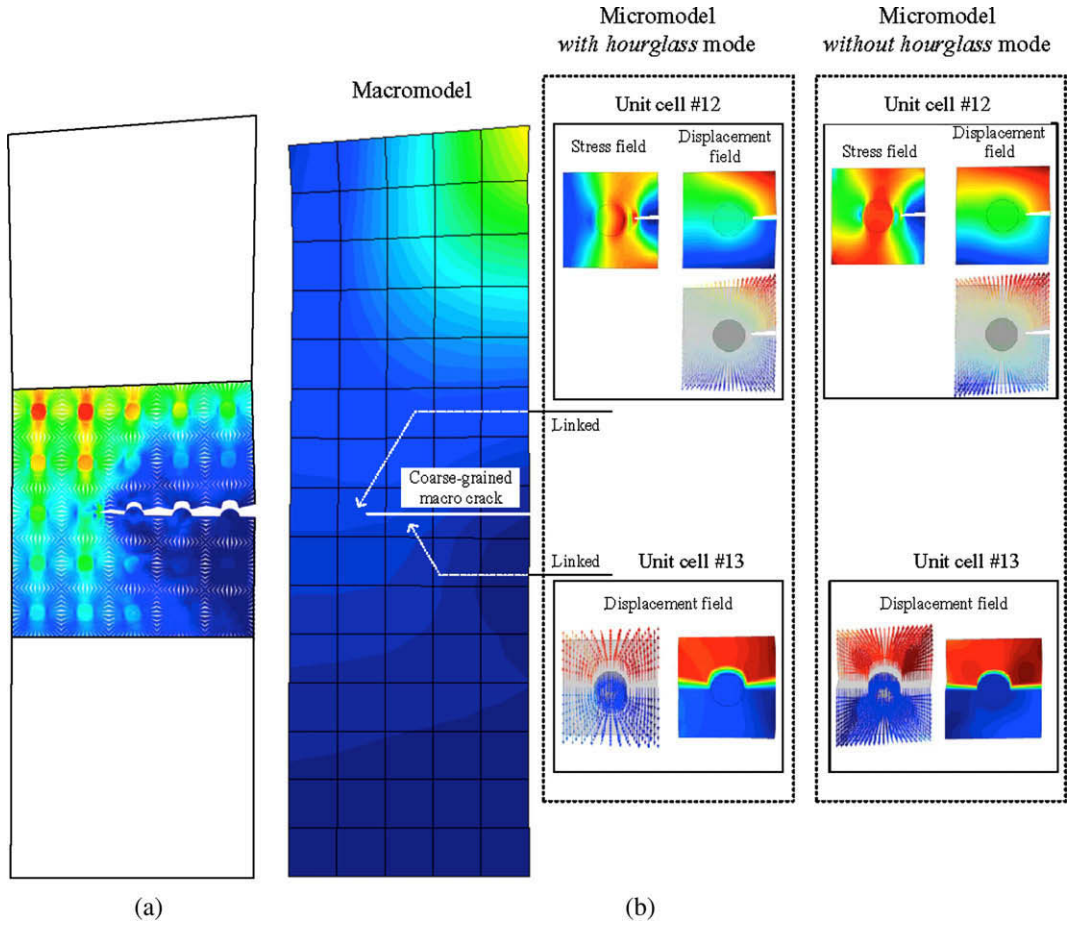

Fig. 10. The evolution of stress and displacement fields, and the path of the crack in: (a) the DNS and (b) the MAD with and without the hourglass mode.

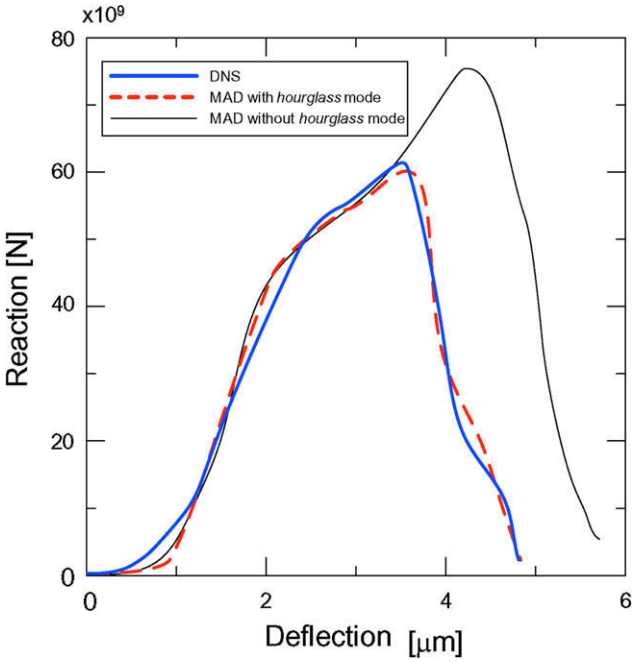

Fig. 11. The comparison of load–deflection curves between the DNS and the MAD with and without the hourglass mode.

$$\boldsymbol{h}^T = [1 \;\; -1 \;\; 1 \;\; -1] \tag{20}$$

$$\begin{bmatrix} \boldsymbol{b}_{xI} \\ \boldsymbol{b}_{yI} \end{bmatrix} = \begin{bmatrix} \partial N_I(\mathbf{0})/\partial x \\ \partial N_I(\mathbf{0})/\partial y \end{bmatrix} \tag{21}$$

The macro stresses are linked to the unit cell as follows. We use the Hill–Mandel energetic relations

$$\delta\mathbf{F}^M : \mathbf{P}^M + \delta\mathbf{q} : \mathbf{Q} = \int_{\Omega_0^m} \mathbf{F}^m : \mathbf{P}^m \mathrm{d}\Omega \tag{22}$$

Substituting the displacement field in Eq. (15) into the above Eq. (22) and assuming that $\mathbf{P}^m$ is an equilibrium field, we obtain the following expressions for the macro stresses

$$\mathbf{P}^M = \frac{1}{\left|\tilde{\Omega}_0^m\right|} \int_{\Gamma_0^m} \mathbf{P}^m \cdot \mathbf{N} \otimes \mathbf{X} \mathrm{d}\Gamma \tag{23}$$

$$\mathbf{Q} = \frac{1}{\left|\tilde{\Omega}_0^m\right|} \int_{\Gamma_0^m} XY\mathbf{P}^m \cdot \mathbf{N} \mathrm{d}\Gamma \tag{24}$$

The expressions for the nodal forces of a four-node quadrilateral element with one-point quadrature and consistent stabilization [18] are then

$$\boldsymbol{f}_{iI}^{int} = \int_{\Omega_0^M} \frac{\partial N_I}{\partial X_j} P_{ij}^M \mathrm{d}\Omega + \boldsymbol{f}_{iI}^{HG} \tag{25}$$

where the hourglass stabilization nodal forces are

$$\boldsymbol{f}_{iI}^{HG} = \mathbf{Q}_i \gamma_I \tag{26}$$

3. Numerical examples

Here, we consider an aluminum–boron composite material to examine the effectiveness of the MAD method. The basic unit cell consists of a boron particle and its surrounding aluminum matrix so that the volume ratio of the boron particles to the aluminum matrix is 10%. We then use the model as a repetitive unit cell for simplicity. The material properties of the aluminum and the boron along with their homogenized material are given in Table 1; for the calculation of the homogenized material properties away from the hot spots, we used a conventional homogenization theory.

3.1. Tests of cell failure modes

The numerical test reported here are quite simplistic since we felt that the only way to evaluate the method was by comparison to direct numerical simulations of models that incorporated the fine-scale features. While it would be desirable to evaluate the method also by comparison to experiments, at this time, data for fine-scale properties, such as fiber–matrix cohesive laws, are quite scarce, so the failure of a computation to agree with experiment would not determine whether it was a shortcoming in the method or the data. Therefore, in the following, the problems all involve comparisons with direct numerical simulations.

The first examples are quasi one dimensional: a long specimen is subjected to an tensile loading but a crack is modeled to grow normal to the loading direction. One objective was to show effectiveness of adding the hourglass mode to unit cell boundary conditions. The models are shown in Fig. 7. A boron particle and aluminum matrix at the center of each specimen is considered.

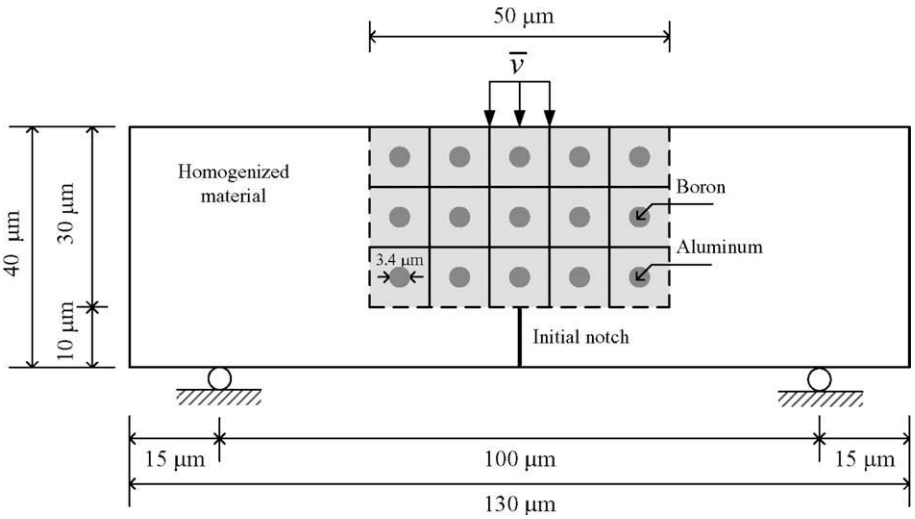

Fig. 12. Initial setup for failure of aluminum–boron composite lamina due to three-point bending.

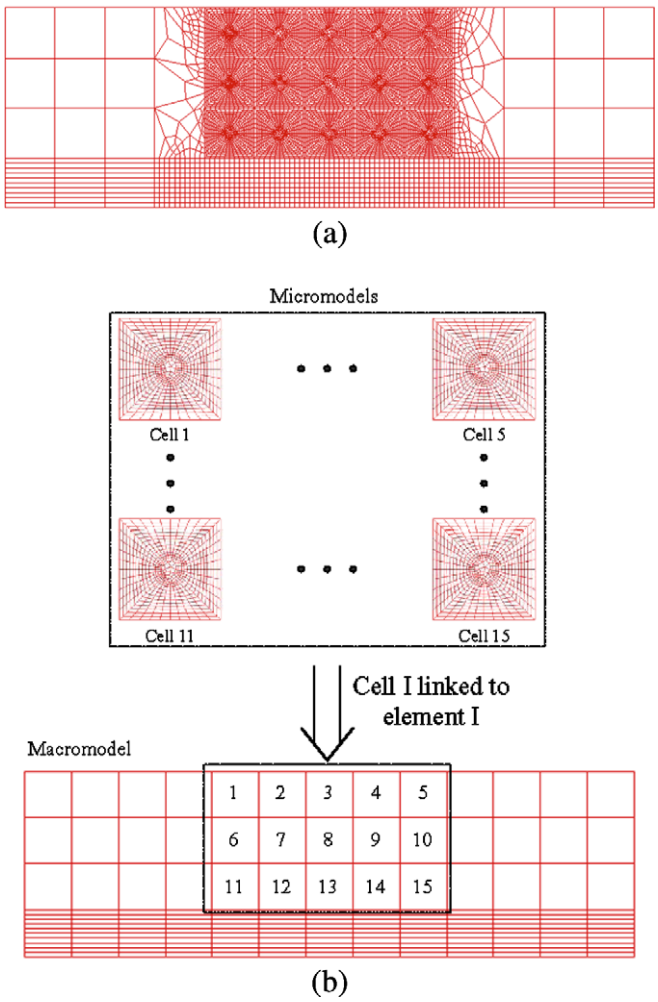

Fig. 13. Finite element discretizations for: (a) the DNS and (b) the coarse model and unit cell models for the MAD method.

The bottom of each specimen is clamped, and at the top of the specimen, we applied two different boundary conditions so that those boundary conditions drive two different failure modes:

(1) in Fig. 7(a), uniform constant velocity is prescribed at the top boundary nodes so that the deformation of the unit cell is almost constant, whereas
(2) in Fig. 7(b), linearly varying velocity is prescribed at the top boundary nodes so that the deformation of the unit cell undergoes bilinear deformation; i.e. the hourglass mode.

In both cases, the prescribed velocities are constant in time.

An initial crack is located at the right edge of the specimen, and it then propagates toward the left edge. For the fracture criterion, we used 3.0% maximum principal tensile strain criterion along with the fracture energy $G_f = 6.0 \times 10^4$ N/m. The discretized fine-scale model for the reference solution by direct numerical simulation (DNS) is shown in Fig. 8(a); its solution is henceforth referred to as the DNS result. The coarse scale model and its linked unit cell model for the MAD method are shown in Fig. 8(b); each finite element is linked with a unit cell.

The load–deflection curves for the prescribed uniform constant velocity boundary condition are shown in Fig. 9; the result for the MAD method *with* the hourglass mode is shown along with that *without* the hourglass mode. As can be seen from Fig. 9, the effect of the hourglass mode in this case is minimal. The results for the MAD methods with and without the hourglass boundary conditions are almost the same. Both results agree with the DNS very closely.

However, when the deformation is such that the bilinear mode is activated in the unit cell boundary conditions, the role of the hourglass mode has a substantial effect. This can be seen from Fig. 10; Fig. 10(a) shows the results for the DNS simulation, and Fig. 10(b) shows the results for the MAD method *with* and *without* the hourglass mode. As shown in Fig. 10(a), the displacement field of the DNS exhibits a bilinear mode, i.e. the hourglass mode, and this bilinear mode is only reproduced in the unit cell when the hourglass mode is considered; see Fig. 10(b). When the hourglass mode is not passed to the finer scale, the fine-scale behavior does not well reproduce the behavior of the DNS model. Without the hourglass mode linkage, the macro model over-predicts the peak load substantially; see Fig. 11.

3.2. Three-point bending beam problem

A second problem we considered, which has substantially more complexity, is the failure of an aluminum–boron lamina in a bending field. We sometimes call this a composite "beam" in three-point bending. We hesitate to use the word "beam" since it does not represent any real composite beam; again, it is toy problem to test the basic methodology by comparison to DNS. The model is shown in Fig. 12. An initial notch is introduced at the center of the bottom surface; the crack propagation at the midspan is mainly in mode I.

For the DNS model, we discretized the beam with 9634 four-node quadrilateral elements as shown in Fig. 13(a). The fine-scale meshing was limited to the center where the failure was expected to progress. The modeling of the center of the beam is quite detailed and requires most of the finite elements for its resolution. For the MAD model, the entire beam was discretized with coarse scale mesh, and the 5×3 elements at the center of the beam are linked to unit cells as shown in Fig. 13(b). Note that the outside

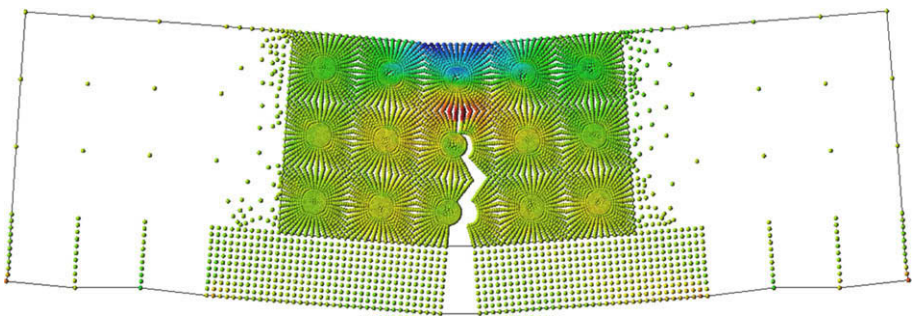

Fig. 14. The path of the crack in the DNS; deformations are magnified by factor of two.

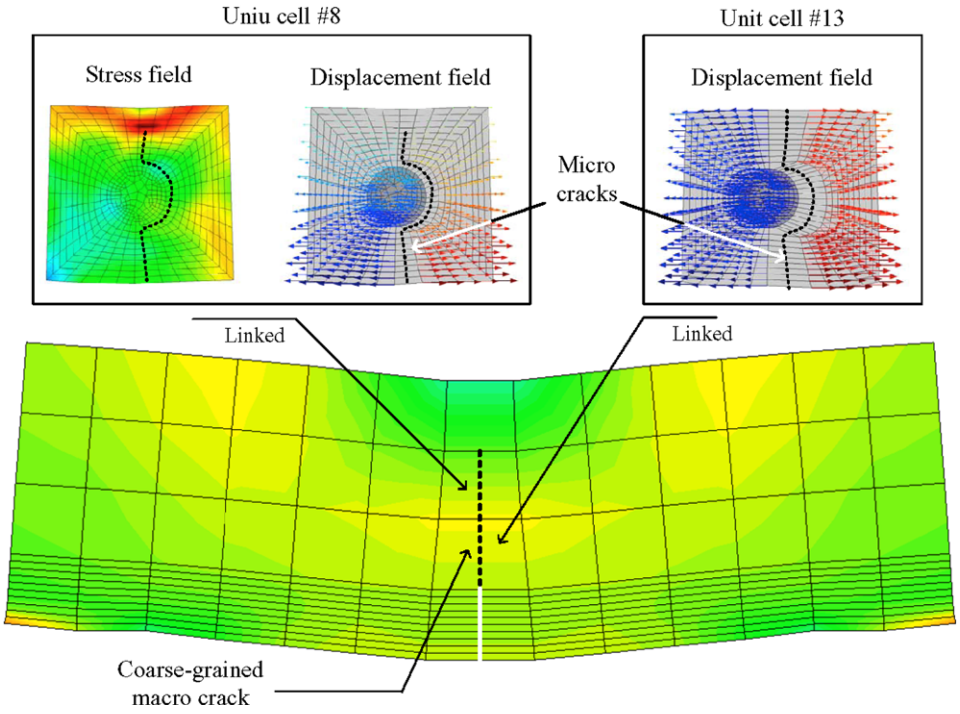

Fig. 15. The result for the MAD method; deformations are magnified by factor of two.

of the center area in both the DNS and the MAD models, we considered a homogeneous material with an effective elastic modulus which is computed by conventional homogenization theory. The material properties are shown in Table 1, and we used a maximum principal tensile strain criterion for fracture of the matrix with a fracture strain of 3.0%; the fracture energy is $G_f = 6.0 \times 10^4$ N/m. The interface stress between the boron fibers were treated by a cohesive law.

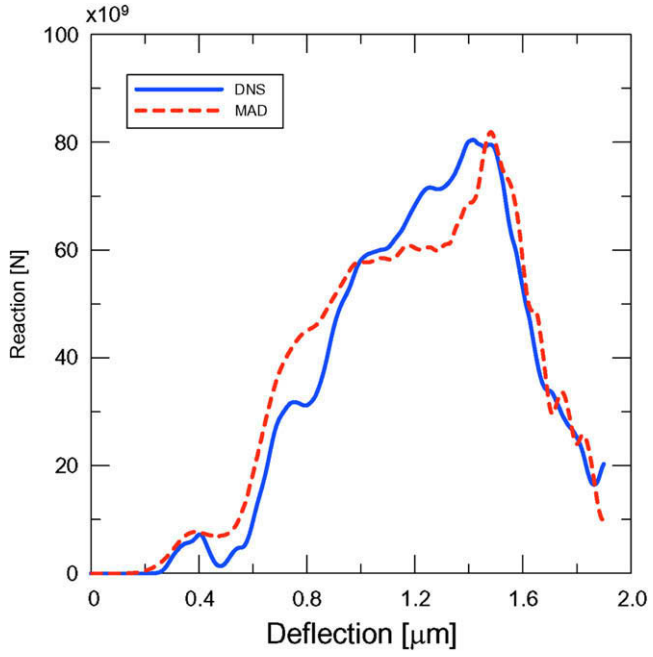

Fig. 16. The comparison of load–deflection curves between the DNS and the MAD with and without the hourglass mode.

Fig. 14 shows the intermediate stage of the crack propagation in the DNS model; in Fig. 14(b). As can be seen from Fig. 14(b), the crack path is quite jagged due to the microstructure; i.e. boron particles.

In the MAD method, such jagged crack paths are only reproduced within the unit cells; equivalent coarse-grained straight cracks are injected to the macro model; see Fig. 15. This is a distinct feature of the coarse graining of the microcracks with the MAD method.

The adequacy of the multiscale solution can be judged from Fig. 16, which compares the load–deflection curves for the MAD to that for the DNS. As can be seen from Fig. 16, there are only some minor discrepancies due in the force–deflection curves computed by the DNS and the MAD methods. However, the overall responses are very similar, and the error in the prediction of the peak load is less than 1%, which is probably fortuitous, since such high accuracy is not expected for coarse-grained models. The coarse-grained model required only 3% of the running time of the DNS model.

4. Conclusions

A study of improved version of the MAD method, a multiscale method for failure analysis, has been presented. This improvement consists of adding an "hourglass mode" to the prescribed displacements of a unit cell. This appears to be particularly advantageous when a unit cell fails by progression of a crack from one edge to the other, which is often the case.

In the MAD method, the microcracking at finer scales is represented by an aggregate, equivalent crack at the coarse scale. The formula for extracting the magnitude and the normal to the equivalent discontinuity at the macroscale is not changed by the addition of the hourglass mode. However additional general stresses and strains are needed at the macroscale. In this paper, we have treated these additional generalized stresses as hourglass forces in the four-node quadrilateral. These can also be incorporated in other elements by adding the bilinear term to the displacement field through meshfree approximations. Another approach we are considering for treating

this mode is a micropolar continuum. However, using classical continuum mechanics for the macroscale bestows significant benefits, so we are inclined to continuing that approach.

As for the original MAD method, the noteworthy features of this improved method are

(1) the decomposition of stable and unstable responses of unit cells by constructing perforated unit cells,
(2) the extraction of a single coarse-grained macro discontinuity from the unstable behavior of the unit cell.

The first feature enables the method to maintain stability of the bulk material. Consequently, the macro material law is stable and remains well-posed. Thus the method should be able to treat failure phenomena by multiscale methods consistently.

The potential and effectiveness of the MAD method have been demonstrated by comparing the results for the MAD method with direct numerical simulations of full fine-scale models of some simple problems. Overall crack paths and predicted peak loads from the MAD method agree quite well with those from the direct numerical simulations, which is encouraging. The running times of the coarse scale models are about 30 times as fast. We are now extending the computer implementations to three dimensions so some comparisons with experiments can be made. The ultimate goal of this work is to apply these methods to three-scale analysis where the finest scale model is atomistic. The material properties, especially the fracture behavior, will then be computed by first principles models.

Acknowledgments

The support of the Army Office of Research under Grant W911NF-05-1-0049 and the Office of Naval Research under Grant N00014-08-1-1191 are gratefully acknowledged.

References

[1] Zohdi TI, Wriggers P. Introduction to computational micromechanics. Lecture notes in applied and computational mechanics, vol. 20. Berlin: Springer; 2005.
[2] Nemat-Nasser S, Hori M. Micromechanics: overall properties of heterogeneous solids. 2nd ed. Amsterdam, New York: Elsevier; 1999.
[3] Feyel F, Chaboche JL. FE^2 multiscale approach for modelling the elastoviscoplastic behaviour of long fiber SiC/Ti composite materials. Comput Meth Appl Mech Eng 2000;183:309–30.
[4] Feyel F. A multilevel finite element method (FE^2) to describe the response of highly non-linear structures using generalized continua. Comput Meth Appl Mech Eng 2003;192:3233–44.
[5] Bažant ZP, Belytschko T. Wave-propagation in a strain-softening bar: exact solution. J Eng Mech ASCE 1985;111:381–9.
[6] Bažant ZP, Belytschko T, Chang TP. Continuum theory for strain-softening. J Eng Mech ASCE 1984;110:1666–92.
[7] Lasry D, Belytschko T. Localization limiters in transient problems. Int J Solids Struct 1988;24:581–97.
[8] Chen Z, Schreyer HL. One-dimensional softening with localization. J Appl Mech Trans ASME 1986;53:791–7.
[9] Kouznetsova V, Geers MGD, Brekelmans WAM. Multi-scale constitutive modelling of heterogeneous materials with a gradient-enhanced computational homogenization scheme. Int J Numer Meth Eng 2002;54:1235–60.
[10] Vernerey FJ, Liu WK, Moran B, Olson G. A micromorphic model for the multiple scale failure of heterogeneous materials. J Mech Phys Solids 2008;56:1320–47.
[11] Vernerey FJ, Liu WK, Moran B. Multi-scale micromorphic theory for hierarchical materials. J Mech Phys Solids 2007;55:2603–51.
[12] Oskay C, Fish J. Eigendeformation-based reduced order homogenization for failure analysis of heterogeneous materials. Comput Meth Appl Mech Eng 2007;196:1216–43.
[13] Fish J, Yuan Z. Multiscale enrichment based on partition of unity. Int J Numer Meth Eng 2005;62:1341–59.
[14] Raghavan P, Ghosh S. Concurrent multi-scale analysis of elastic composites by a multi-level computational model. Comput Meth Appl Mech Eng 2004;193:497–538.
[15] Ghosh S, Bai J, Raghavan P. Concurrent multi-level model for damage evolution in micro structurally debonding composites. Mech Mater 2007;39:241–66.
[16] Belytschko T, Loehnert S, Song JH. Multiscale aggregating discontinuities: a method for circumventing loss of material stability. Int J Numer Meth Eng 2008;73:869–94.
[17] Belytschko T, Song JH. Coarse graining of multiscale crock propagation. Int J Numer Meth Eng, accepted for publication.
[18] Flanagan DP, Belytschko T. A uniform strain hexahedron and quadrilateral with orthogonal hourglass control. Int J Numer Meth Eng 1981;17:679–706.
[19] Belytschko T, Ong JSJ, Liu WK, Kennedy JM. Hourglass control in linear and nonlinear problems. Comput Meth Appl Mech Eng 1984;43:251–76.
[20] Belytschko T, Bachrach WE. Efficient implementation of quadrilaterals with high coarse-mesh accuracy. Comput Meth Appl Mech Eng 1986;54:279–301.
[21] Belytschko T, Black T. Elastic crack growth in finite elements with minimal remeshing. Int J Numer Meth Eng 1999;45:601–20.
[22] Moes N, Dolbow J, Belytschko T. A finite element method for crack growth without remeshing. Int J Numer Meth Eng 1999;46:131–50.
[23] Song JH, Areias PMA, Belytschko T. A method for dynamic crack and shear band propagation with phantom nodes. Int J Numer Meth Eng 2006;67:868–93.
[24] Belytschko T, Lu YY, Gu L. Element-free Galerkin methods. Int J Numer Meth Eng 1994;37:229–56.